ELSEVIER

Geotextiles and Geomembranes 16 (1998) 1–25

Geotextiles and Geomembranes

Variational displacement method for geosynthetically reinforced slope stability analysis: I. Local stability

P. Lemonnier[a], A.H. Soubra[b], R. Kastner[c]

[a] *Aalborg University, Department of Civil Engineering, Aalborg, Denmark*
[b] *Ecole Nationale Supérieure des arts et Industries, Strasbourg, France*
[c] *Institut National des Sciences Appliquées, Villeurbanne, France*

Abstract

This, and a companion paper (Lemonnier et al., 1998), present a theoretical model, allowing the assessment of the safety factor of a geosynthetically reinforced slope. The present paper deals with the local stability problem, that is the determination of tension and strain distributions in the reinforcements. The global stability analysis of the reinforced slope, which includes this local stability analysis for each sheet of reinforcement, is described in the companion paper. As an improvement of the French 'displacement method', (Gourc et al., 1986), the present theoretical model for the local stability analysis is based on the anchored membrane concept. Its originality is the use of the variational calculus applied to the equilibrium of the membrane. It allows the determination of the optimal shape of the membrane, which gives the minimal tension at the failure surface. This optimal shape has been found to be a log-spiral. A numerical study shows the influence of several geometrical parameters on the determination of the reinforcement tension. Finally, a case history comparison involving results obtained from six current design methods is presented and discussed. © 1998. Published by Elsevier Science Ltd.

Keywords: Slopes; Reinforced soil; Analysis; Stability

1. Introduction

The problem of internal and external stability is one of the most important in the design and analysis of geosynthetic reinforced soil slopes. The internal stability includes the rupture of reinforcement and pullout failure. The external stability includes sliding, overturning, bearing capacity and overall stability. The majority of

S0266-1144/98/$19.00 © 1998. Published by Elsevier Science Ltd.
PII S0266-1144(97)10020-6

methods available in literature concerning the determination of the safety factor against failure are based on lateral earth pressure considerations (Steward et al., 1977; Broms, 1978; Collin, 1986; Bonaparte et al., 1987) or employ the approach commonly used in conventional slope stability analysis, modified to account for the inclusion of the tension in the reinforcements (Blanchier, 1982; Leshchinsky and Reinschmidt, 1985; Delmas et al., 1986; Hird, 1986; Huisman, 1987; Low et al., 1990; Kaniraj, 1994). The latter methods have used different assumptions concerning the magnitude and the inclination of the reinforcement tension at the failure surface. The different directions that have been assumed by some investigators are (1) horizontal (Leshchinsky and Reinschmidt, 1985; Delmas et al., 1986; Hird, 1986), (2) tangential to the failure surface (Delmas et al., 1986), (3) in the direction of the bisector to the horizontal and the tangential directions (Huisman, 1987; Low et al., 1990; Kaniraj, 1994) and (4) orthogonal to the radius of the log-spiral slip surface (Leshchinsky and Reinschmidt, 1985).

Furthermore, there is a number of other design methods available for geosynthetic reinforced slopes based on a displacement approach. These methods have considered a prescribed displacement at the top of the slope in order to mobilise the tensions in the reinforcements. The original method, called the 'displacement method' (Gourc et al., 1986), is being widely used in France and in several other countries for the design of such structures. The use of this method to estimate the failure limit state of such structures can now be considered to give satisfactory results. Geotechnical engineers have built up this reliance from several experimental investigations and theoretical validations all over the world (GourGourc et al., 1992; Gourc et al., 1992; Yoshioka et al., 1990; Delmas et al., 1992; Fidler et al., 1994). This method is based on the principle of soil limit equilibrium, associated with the anchored membrane behaviour of the geosynthetic reinforcement. The original method ('Cartage' French software) considered a simplified mechanism for this membrane (rectilinear shape). Later on, a more rigorous mechanism (circular shape) was proposed. The advantage of this method is its ability to take into account the extensibility of the reinforcements in the design, which is a major characteristic of geosynthetics. Also, it allows one to take into account the complex soil–geotextile interaction mechanism that actually occurs, and one can check the soil–reinforcement strain compatibility.

In this paper, an extension of the 'displacement method' presented by Gourc et al. (1986) is proposed. It allows the determination of the geometry of the membrane, which gives the minimum value of the tension in the reinforcement at the failure surface and simultaneously satisfies the three static equilibrium equations of this membrane using a variational approach. In the following section, the 'displacement method' given by Gourc et al. (1986) is briefly reviewed, and then the present variational formulation is presented.

2. Determination of the tension in the reinforcement

This study takes place in the general framework of geotextile reinforced slope stability analysis. Fig. 1 shows a geosynthetic reinforced slope inclined at β (with the

horizontal direction). This paper only considers the determination of tension T_i in the reinforcement i at the intersection with the failure surface $Y(X)$ (see Fig. 1).

As mentioned above, Gourc et al. (1986) have suggested a displacement approach and have considered an anchored membrane in the neighbourhood of the failure surface (see Fig. 2). They have made assumptions concerning the magnitude and the direction of the uniform pressure distribution, p, applied to this membrane. These authors have shown that the assumed distributions lead to a membrane that has the form of a circle or a hyperbola, and to a constant tension in the membrane.

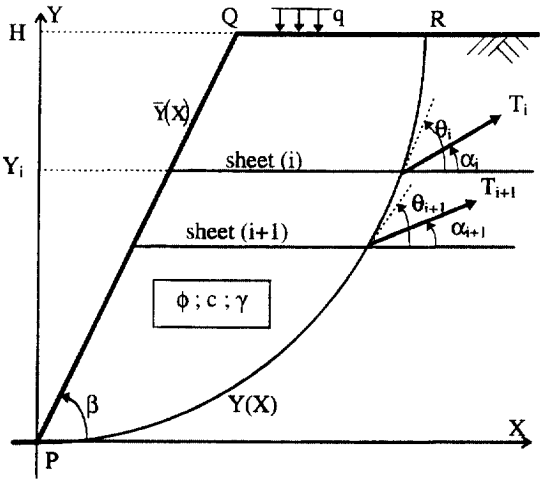

Fig. 1. Geotextile reinforced slope stability analysis.

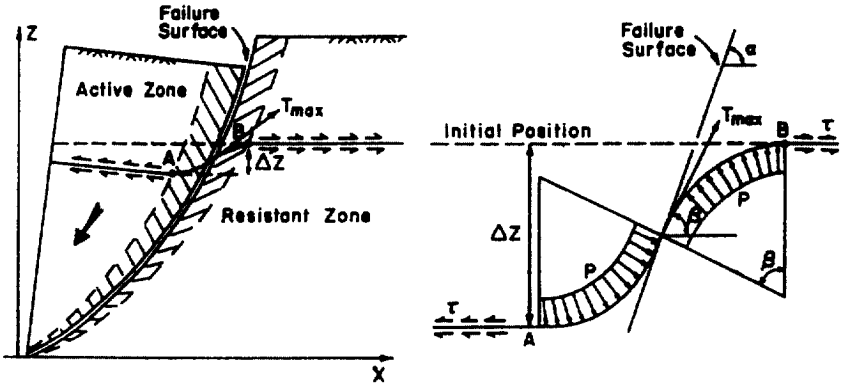

Fig. 2. Anchored membrane concept for geotextile reinforcement (Gourc et al., 1986).

In this paper, a new method for the determination of the reinforcement tensions is proposed. It is based on the following assumptions:

- The total membrane B_1B_2 (see Fig. 3) is assumed to be symmetrical with respect to point A. This is in conformity with published results from model tests (Galera, 1990). Thus, tension T_A in the geotextile sheet at point A, is determined by means of the equilibrium of a half membrane,
- The location of maximum tension in the reinforcement coincides with the failure surface,
- Tension T_A is assumed to be tangential to the membrane since the reinforcement has no flexion rigidity,
- The mechanical behaviour of the soil–reinforcement interface is characterised by a friction angle ϕ_g and an adhesion c_g that are assumed to be constant on both sides of the reinforcement. These parameters should be determined by soil–geosynthetic direct shear tests.

The present method includes the four following points (see Fig. 3):

1. Application of the variational calculus to the equilibrium of upstream membrane AB_1 (upstream refers to the failure surface). It allows the determination of the extreme shape of the membrane AB_1 that (1) minimises tension T_A, and (2) satisfies simultaneously the three static equilibrium equations of the membrane. This will lead to a relationship between the tension forces at points A and B_1 (i.e. T_A and T_{B1}).
2. Determination of tension T_{B1}, using the tension–displacement relationship of the anchorage B_1F. This relationship allows the determination of the tensions T and the relative soil–geotextile displacements u at any point of the anchorage as functions of u_F (relative displacement at point F). This calculation scheme is based on the work of Gourc et al. (1986);
3. Determination of unique solution for u_F value, and consequently for T_A, using the displacement compatibility equation of the upstream zone.

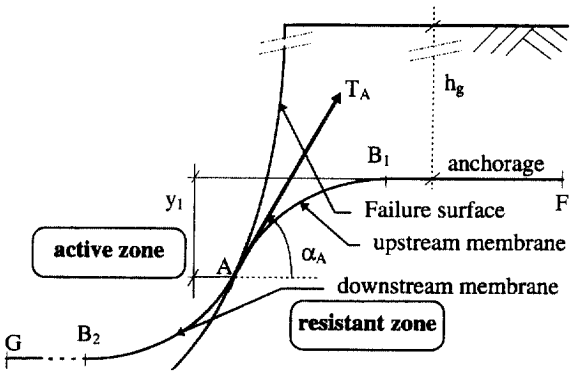

Fig. 3. Anchored membrane. Notations.

4. Equilibrium of the downstream membrane in order to check the validity of the solution with respect to the failure by breakage or sliding of the reinforcement.

Note that points 1, 3 and 4 are new considerations, whereas point 2 is part of the existing 'displacement method'. These four points are detailed in the following sections.

2.1. *Variational approach applied to the membrane*

As shown in Fig. 3, a geosynthetic reinforcement is placed at a depth h_g below the ground surface, and subjected to a known vertical displacement y_1 at point A. Note that, for the purpose of clarity, the representation of y_1 in Fig. 3 is exaggerated.

B_1, B_2 are the unknown points of the reinforcement that separate the anchored and membrane zones. Thus, the two zones GB_2 and B_1F, which behave as anchorages, remain horizontal, whereas the zone B_2B_1, which behave, as a membrane, gets an unknown shape. In the following, we are looking for the shape of this membrane that gives the minimum value of the reinforcement tension at the failure surface. The justification of such a statement is that when a state of limit equilibrium is reached, the upstream membrane AB_1 and the neighbouring soil deform in such a manner to attain the least lateral pressure as possible by developing the active zone, that is to mobilise the minimum value of T_A.

Thus, the problem is to assess the unknown tension force T_A (magnitude and direction: T_A, (α_A). As shown in Fig. 4, upstream membrane AB_1 is described by an unknown function $y(x)$ in the (A, x, y) coordinate system. It is subjected to tension T_A at point A, to tension T_{B1} at point B_1 and finally to normal and tangential stress distributions σ_1 and τ_1 (resp. σ and τ) on the upper (resp. lower) face of the membrane. The equilibrium equations are given as follows:

- Horizontal equilibrium:

$$T_A \cos \alpha_A = T_{B_1} + \int_0^{\ell} (\tau \cos \zeta - \sigma \sin \zeta)\, ds + \int_0^{\ell} (\tau_1 \cos \zeta + \sigma_1 \sin \zeta)\, ds \qquad (1.1)$$

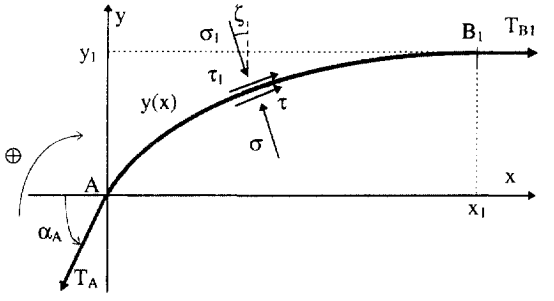

Fig. 4. Free body diagram of upstream membrane AB_1.

- Vertical equilibrium:

$$T_A \sin \alpha_A = \int_0^{\ell} (\tau_1 \sin \zeta - \sigma_1 \cos \zeta)\, ds + \int_0^{\ell} (\tau \sin \zeta + \sigma \cos \zeta)\, ds \tag{1.2}$$

- Moment equilibrium around point A:

$$T_{B_1} y_1 = \int_0^{\ell} [((\sigma - \sigma_1) \sin \zeta - (\tau - \tau_1) \cos \zeta) y + ((\tau + \tau_1) \sin \zeta + (\sigma - \sigma_1) \cos \zeta) x]\, ds, \tag{1.3}$$

where $\zeta = \zeta(s)$ represents the inclination of the membrane at point M to the horizontal direction, (x_1, y_1) are the coordinates of point B_1 in the local (A, x, y) reference system, s is the curvilinear coordinate of point M, and ℓ is the length of the membrane (i.e. AB_1).

Note that tension T_{B1}, which appears in these equations, is determined through the equilibrium of the upstream anchored zone B_1F (see Fig. 3) as will be shown later. Furthermore, one assumes that a state of limit equilibrium is reached for the soil–membrane interface and that the Mohr–Coulomb criteria are satisfied on both sides of the membrane.

$$\begin{aligned} &\tau = \sigma tg\phi_g + c_g \\ &(\tau_1 = \sigma_1 tg\phi_g) + c_g \end{aligned} \tag{2}$$

The quantity T_A required to bring the soil–membrane interface to a state of limit equilibrium depends on the choice of the three functions $y(x)$, $\sigma(x)$ and $\sigma_1(x)$. Note that the friction on this membrane is mostly mobilised on the concave face (i.e. on the lower face of this membrane). Therefore, the authors think that it would be dangerous to make any assumptions concerning the normal stress distribution on this face [i.e. $\sigma(x)$]. However, the normal stress distribution σ_1 on the upper face of the membrane is essentially due to the soil weight above this membrane. Hence, T_A necessarily depends on depth h_g (see Fig. 3). Now, this term does not appear in the equilibrium equations (Eqs. (1.1,1.2,1.3,2), (1.2,1.3,2), (1.3,2) and (2)). Thus, in order to relate T_A to h_g, four different assumptions (namely models 1–4) concerning the σ_1 distribution are made. They are defined as follows:

1. Model 1: One assumes that σ_s, the resultant of the elementary stresses σ_1 and $\sigma_1 tg\phi_g$ equals soil weight above the membrane (see Fig. 5):

$$\sigma_s = \gamma h + q$$

where γ represents the effective unit weight of the soil, h the height of soil above point M, and q the uniformly distributed normal surcharge at the top of the reinforced slope. Thus, σ_1 stress can be written as follows:

$$\sigma_1 = (\gamma h + q).\cos \phi_g \tag{3}$$

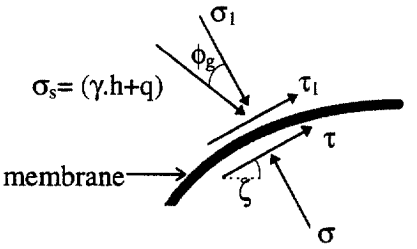

Fig. 5. Model 1 for σ_1 distribution.

2. Model 2: The magnitude of the normal stress is expressed as follows:

$$\sigma_1 = (\gamma h + q)\cos^2\zeta \tag{4}$$

This expression of σ_1 is sometimes called the 'Fellenius stress' in the slope stability analysis. Indeed, it refers to the equilibrium of a vertical slice of soil whose base is inclined at ζ to the horizontal direction, assuming that interslice forces are parallel to the base of each slice. Fig. 6 shows the normal stress σ_1 and the resultant stress σ_s as defined in model 1.

3. Model 3: This model is the one proposed by Faure (1986) in his slope stability analysis method. The principal directions are assumed to be the horizontal and vertical ones. The principal stresses are thus expressed as follows:

$\sigma_v = \gamma h + q$ on a horizontal facet

σ_h unknown on a vertical facet

Then, the normal stress σ_1 that acts on a facet inclined with an angle ζ to the horizontal direction, can be assessed by a simple construction of the Mohr's circle. It can be written as follows:

$$\sigma_1 = \frac{\gamma h + q}{2}\left[(1 + \cos 2\zeta) + \frac{1 - \cos 2\zeta}{tg^2\left(\frac{\pi}{4} + \frac{\phi_g}{2}\right)}\right] + \frac{c_g(\cos 2\zeta - 1)}{tg\left(\frac{\pi}{4} + \frac{\phi_g}{2}\right)} \tag{5}$$

4. Model 4: This model is based on the assumption of Bishop concerning inter-slice forces in his slope stability analysis method. The normal stress σ_1, which acts on a base of a slice inclined with an angle ζ to the horizontal direction, corresponds to the equilibrium of a vertical slice of soil whose inter-slice shear forces are neglected. Thus, the following expression is obtained:

$$\sigma_1 = \frac{\gamma h - c_g tg\zeta + q}{1 + tg\phi_g tg\zeta} \tag{6}$$

In the following, the variational calculus is applied to the equilibrium of the upstream membrane AB_1 considering model 1, then the obtained results will be extended to the three other models.

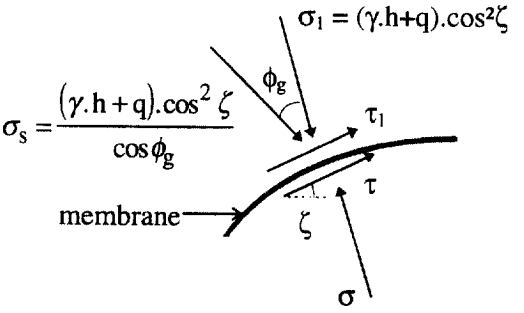

Fig. 6. Model 2 for σ_1 distribution.

2.1.1. Variational approach—Model 1

The normal stress distribution σ_1 is given by Eq. (3). The depth h of soil above M can be expressed in the local (A, x, y) coordinate system (see Figs. 3 and 4) as follows:

$$h = h_g + y_1 - y \tag{7.1}$$

Furthermore, one can write

$$y' = tg\,\zeta \tag{7.2}$$

and

$$ds = \frac{dx}{\cos\zeta}. \tag{7.3}$$

Substituting Eqs. (2) and (3) into Eqs. (1.1,1.2,1.3), (1.2,1.3) and (1.3), taking into account Eqs. (7.1,7.2,7.3), (7.2,7.3) and (7.3), three limit equilibrium equations of the upstream membrane can be expressed as follows:

$$T_A \cos\alpha_A = T_{B_1} + \int_0^{x_1}\left[2c_g + \sigma(tg\phi_g - y') + k[\gamma(h_g + y_1 - y) + q] \times \frac{\sin(\zeta + \phi_g)}{\cos\zeta}\right]dx \tag{8.1}$$

$$T_A \sin\alpha_A = \int_0^{x_1}\left[2c_g y' + \sigma(tg\phi_g.y' + 1) - k[\gamma(h_g + y_1 - y) + q] \times \frac{\cos(\zeta + \phi_g)}{\cos\zeta}\right]dx \tag{8.2}$$

$$-T_{B1}y_1 = \int_0^{x_1}\left\{k.[\gamma.(h_g + y_1 - y) + q]\left[\frac{\sin(\zeta + \phi_g)}{\cos\zeta}y + \frac{\cos(\zeta + \phi_g)}{\cos\zeta}x\right] + [2c_g + \sigma.(tg\,\phi_g - y')]y - [2c_g y' + r.(tg\,\phi_g - y' + 1)]x\right\}dx. \tag{8.3}$$

Note that T_A appears in the two equilibrium Equations (8.1) and Eq. (8.2). This tension may be expressed from one of these equations, in terms of the two functions $y(x)$ and $\sigma(x)$. The quantity T_A, for which the membrane attains a state of limit equilibrium, depends in general on the kinematical and the statical functions $y(x)$ and $\sigma(x)$, respectively. Therefore, T_A is a functional of two functions. This functional is termed the tension functional, and the critical tension $T_{A\text{mini}}$ is the minimum value of T_A:

$$T_{A\text{mini}} = \min_{y,\sigma} T_A\{y(x); \sigma(x)\} = T_A[y_e(x), (\sigma_e(x)],$$

where $y_e(x)$ [resp. $\sigma_e(x)$] defines the critical shape of the membrane (resp. the critical normal stress distribution). The problem of the equilibrium of the membrane can now be stated as follows: find a pair of functions $y_e(x)$ and $\sigma_e(x)$ that realises the minimum value $T_{A\text{mini}}$ (critical tension) of the tension functional T_A, such that the three limit equilibrium equations (Eqs. (8.1,8.2,8.3), (8.2,8.3) and (8.3)) are satisfied. This problem is solved using variational calculus as proposed by Baker and Garber (1977) in the case of unreinforced slope stability analysis. The calculus is briefly presented here. The reader can find more details elsewhere (Lemonnier, 1995).

The terms $\cos\alpha_A$ and $\sin\alpha_A$ that appear, respectively, in Eq. (8.1) and (8.2), give the tension functional a particular property: its dependence on y'_0, which represents the slope of the membrane at point A. Indeed, if we choose Eq. (8.2) to define the functional, the problem can be expressed as follows:

$$\min T_A = \int_0^{x_1} \left\{ \sqrt{\frac{1+y_0'^2}{y_0'^2}} \left[2c_g y' + \sigma(tg\phi_g y' + 1) - [\gamma(h_g + y_1 - y) + q] \times \frac{\cos(\zeta + \phi_g)}{\cos\zeta} \right] \right\} dx \tag{9.1}$$

subject to the two following constraints:

$$\int_0^{x_1} \left[2c_g + \sigma_e(tg\phi_g - y'_e) + [\gamma(h_g + y_1 - y_e) + q] \frac{\sin(\zeta + \phi_g)}{\cos\zeta} \right] dx = T_{A\text{mini}} \cos\alpha_{Am} - T_{B_1} \tag{9.2}$$

$$\int_0^{x_1} \left\{ \begin{array}{l} [\gamma(h_g + y_1 - y_e) + q] \left[\dfrac{\sin(\zeta + \phi_g)}{\cos\zeta} y_e + \dfrac{\cos(\zeta + \phi_g)}{\cos\zeta} x \right] + \\ [2c_g + \sigma_e(tg\phi_g - y'_e)] y_e - [2c_g y'_e + \sigma_e(tg\phi_g - y'_e + 1)] x \end{array} \right\} dx = -T_{B_1} y_1, \tag{9.3}$$

where the angle α_{Am} corresponds to the inclination of $T_{A\text{mini}}$, that is to the critical position. Eqs. (9.2) and Eq. (9.3), which are the integral constraints, are derived from

Eqs. (8.1) and (8.3), respectively. The tension functional can be reduced to the following form:

$$J = \int_0^{x_1} T_A(x, y, y'_0, y', \sigma)\,\mathrm{d}x$$

Note that one endpoint of the functional is null, and the other (i.e. x_1) is variable. Furthermore, the two integral constraints are of the following type:

$$\int_0^{x_1} k_i(x, y, y', y'_0, \sigma) = \chi_i \quad \forall i \in \{1, 2, 3\},$$

where k_i and χ_i are obtained by identification. Thus, this problem is a standard isoperimetric one with a variable endpoint. The solution to this problem can be obtained using the method of Lagrange's undetermined multipliers. Following the same procedure as in Baker and Garber (1977), an auxiliary function R may be introduced as follows: $R = F + (_1 K_1 + \lambda_2 K_2$, where F, K_1, K_2 are intermediate functions.

Therefore, the functions $y_e(x)$ and $\sigma_e(x)$ that constitute the solution to the problem have to satisfy the following conditions:

1. Two Euler differential equations for the function R, namely:
   First equation:

$$R_{\sigma_e} - \frac{\mathrm{d}}{\mathrm{d}x} R\sigma'_e = 0 \tag{10.1}$$

   Second equation:

$$R_{y_e} - \frac{\mathrm{d}}{\mathrm{d}x} R y'_e = 0 \tag{10.2}$$

2. Two integral constraints (Eqs. (9.2,9.3) and (9.3)).
3. Two boundary conditions for each end-point:
   - fixed end-point A: $x = 0$ and $y = 0$.
   - variable end-point B_1: $x = x_1$. For this type of end-point, a variational boundary condition, known as the transversality condition, is to be satisfied.

2.1.1.1. First Euler equation.

R is independent of σ'_e and dependent on σ_e (cf. Eqs. (9.1,9.2,9.3), (9.2,9.3) and (9.3)), the first Euler equation (Eq. (10.1)) is a first-order differential equation in y_e only. Solving this equation in terms of polar co-ordinates (r_g, θ_g), one obtains

$$r_g = r_{g_0} \cdot \mathrm{e}^{(\theta_{g_0} - \theta_g) \operatorname{tg} \phi_g}. \tag{11}$$

Eq. (11) represents the equation of log-spirals of angle ϕ_g, with pole at (x_c, y_c) (see Fig. 7).

As shown in Fig. 7, r_g decreases when angle θ_g increases, for $\phi_g \neq 0$. In case of $\phi_g = 0$, r_g remains constant when θ_g varies; thus, one obtains, in this case, a circle

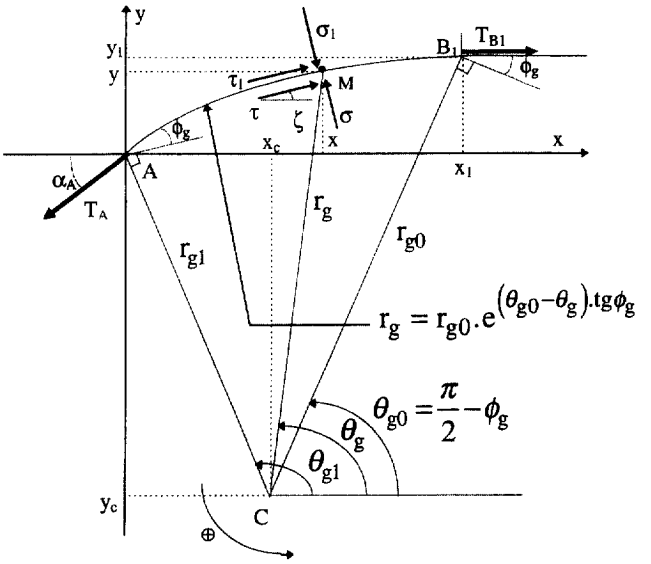

Fig. 7. Shape of the upstream membrane from the present variational analysis.

whose radius is r_{g_0}. At point B_1, the tangent to the membrane remains in the horizontal direction. This condition implies that angle θ_{g_0} is constant and equals $(\pi/2 - \phi_g)$. Consequently, the family of possible critical shapes of the membrane is the one of log-spirals, which are defined by only one parameter, i.e. angle θ_{g1}. Furthermore, note that the log-spiral has a particular geometrical property, that the resultant of the elementary forces ($\sigma\, ds$) and ($tg\phi_g \sigma\, ds$) passes through the pole C of the spiral. Hence, the moment equation about the pole is independent of the stress distribution $\sigma(x)$ and may be used for the determination of the critical tension T_{Amini}. The two remaining equilibrium equations may be satisfied by every $\sigma(x)$ distribution that has two degrees of freedom. Thus, one may find the critical θ_{g1} value that simultaneously satisfies the moment equation (Eq. (12.1)) and gives the minimum value of T_A (Eq. (12.2)). This is done by a one-dimensional minimisation procedure of T_A with respect to θ_{g1}.

$$\sum m_{/c}(\theta_{g1}) = 0 \rightarrow T_A = T_A(\theta_{g1}, T_{B1}) \tag{12.1}$$

$$T_{Amini} = \min_{\theta_{g1}} (T_A). \tag{12.2}$$

2.1.1.2. Second Euler and transversality equations.

Since the aim of this study is the determination of the critical tension and its inclination, the results obtained so far are sufficient to solve the problem. Indeed, it has been shown by Baker and Garber (1977), in the case of unreinforced slope stability

analysis, that the second Euler and the transversality equations give the normal stress distribution $\sigma(x)$. In the present analysis, it is also the case, but since the $\sigma(x)$ distribution is not necessary to assess T_{Amini} and α_{Am}, we will not express these equations.

2.1.2. Variational approach—Other models

Let us note σ_1^i the σ_1 distribution corresponding to model i ($i = 1, 2, 3$ or 4), then Eqs. (3)–(6) may be expressed as follows:

$$\sigma_1^{(i)} = s_i(\gamma h + q)\cos\phi_g,$$

where

$$s_1 = 1$$

$$s_2 = \frac{\cos^2\zeta}{\cos\phi_g}$$

$$s_3 = \frac{1}{2\cos\phi_g}\left[1 + \cos 2\zeta + \frac{1 - \cos 2\zeta}{tg^2\left(\frac{\pi}{4} + \frac{\phi_g}{2}\right)} + \frac{c_g(\cos 2\zeta - 1)}{tg\left(\frac{\pi}{4} + \frac{\phi_g}{2}\right)(\gamma h + q)}\right]$$

$$s_4 = \frac{(\gamma h + q) - c_g tg\zeta}{\cos\phi_g(\gamma h + q)(1 + tg\phi_g\, tg\zeta)}.$$

Thus, by multiplying σ_1 corresponding to model 1, by a coefficient s_i defined above, one obtains $\sigma_1^{(i)}$ corresponding to model i. However, these coefficients depend on $y(x)$ and $y'(x)$ (through h and ζ, respectively), but are independent of the $\sigma(x)$ distribution. Consequently, since the first Euler equation concerns the partial derivative of the functional with respect to $\sigma(x)$, one can easily show that the variational calculus applied to the three other models gives the same conclusions obtained for model 1. Nevertheless, the critical tension is not the same for each model.

2.2. Equilibrium of the downstream membrane

As mentioned above, membrane AB_2 is assumed to be symmetrical to AB_1 with respect to point A. Thus, membrane AB_2 is subjected to (see Fig. 8): critical tension T_{Amini}; tension T_{B2}, which remains horizontal; normal and tangential stress distributions σ_2 and τ_2 (resp. σ' and τ') on the lower (resp. upper) face of the reinforcement.

Furthermore, the following assumptions for zone AB_2 will be adopted here:

1. A state of limiting equilibrium is assumed to occur on both faces of downstream membrane AB_2, that is:

$$\tau' = \sigma' tg\phi_g + c_g$$
$$\tau_2 = \sigma_2 tg\phi_g + c_g \qquad (13)$$

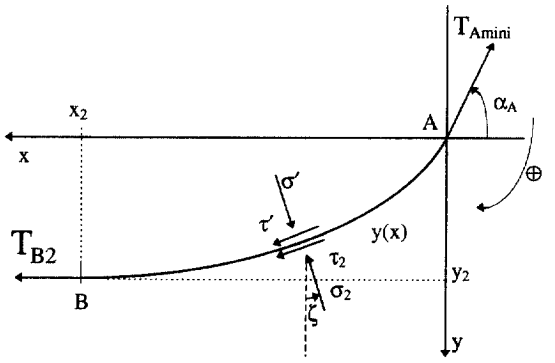

Fig. 8. Free body diagram of downstream membrane AB_2.

2. The interface friction is mostly mobilised on the concave face of the membrane, that is on its upper face. Thus, no assumption will be made for the σ' distribution.
3. Concerning σ_2 distribution, an assumption is presently made in order to simplify the resolution: it is assumed to be null, that is the membrane decollates at its lower face.

Note that the two first points are the same as for zone AB_1, whereas point 3 is different.

Thus, writing the only moment equilibrium equation about the pole of the known log-spiral defining AB_2 zone, one obtains T_{B2} without any assumptions concerning normal stress distribution $\sigma'(x)$. For the same reason as for the upstream membrane, the two other force equilibrium equations are implicitly satisfied.

2.3. *Tension–displacement relationship of the anchorage*

To determine the tensions in the anchorage, one considers the model of the soil–geotextile interaction proposed by Gourc et al. (1986). It is based on the following two relationships (see Fig. 9):

1. A linear elastic tension–strain relationship for the geotextile:

$$T = J\varepsilon, \tag{14}$$

where T is the tension force, J the tensile stiffness and ε the strain in the geotextile;
2. An elasto-plastic relationship for the friction behaviour of the soil–geotextile interface:

$$\tau = \begin{cases} \lambda u & \text{if } u < u_p \\ \tau_p & \text{if } u \geqslant u_p \end{cases} \tag{15}$$

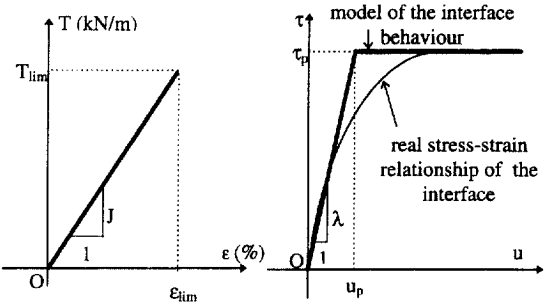

a) Tension-strain relationship of the geotextile.

b) Stress-displacement relationship of the soil-geotextile interface.

Fig. 9. Tensile and friction behaviour of the inclusion.

where τ is the mobilised shear stress at any point M of the interface, u the relative soil-reinforcement displacement at this point, λ the slope of the straight line that characterises the elastic behaviour of the interface, τ_p the ultimate shear stress and u_p the minimum value of u that mobilises τ_p (see Fig. 9(b)). The relative displacement u_p should be determined by a laboratory friction test.

Thus, considering that a state of limiting equilibrium is reached on both soil–geotextile interfaces, the Mohr–Coulomb criterion has to be satisfied:

$$\tau_p = \sigma_n tg\phi_g + c_g \tag{16}$$

Combining Eq. (14) with Eqs. (15) and (16) for each anchorage zone, one obtains two relationships giving the displacement u and the tension T at any point of the anchorage for a prescribed boundary condition at point G (see Fig. 3). This boundary condition may be either: (1) free anchorage where $T_G = 0$ and $u_G \neq 0$, or (2) fixed anchorage where $T_G \neq 0$ and $u_G = 0$. Let us consider the free anchorage; then these relationships may be reduced as

$$T_{B_1} = f(u_F), \tag{17.1}$$

$$T_{B_2} = f(u_G) \tag{17.2}$$

Note that zones GB_2 and B_1F (see Fig. 3) are characterised by the rates of linear behaviour of these zones (called ta_G and ta_F, respectively). These rates are defined as the ratio of the length of the portion that behaves linearly (called x_{pG} and x_{pF}, respectively) over the total length of the anchorage for each zone (B_1F and GB_2, respectively):

$$ta_F = \frac{xpF}{B_1F}$$

$$ta_G = \frac{x_{pG}}{GB_2}$$

These computed rates (ta_G and ta_F) have to be larger than a minimum value ta_{mini} prescribed by the designer:

$$ta_F > ta_{mini}$$

$$ta_G > ta_{mini}$$

These conditions assure the non-failure of the geotextile reinforcement by lack of adherence (sliding of the sheet).

2.4. Displacement compatibility

The analysis done so far leads to a problem with one degree of freedom. That is, the critical tension and its inclination depend on the relative displacement u_F (cf. Eqs. (12.1,7.1) and (17.1)). The missing equation is the one that allows the satisfaction of the displacement compatibility for the zone AF of the geotextile. Indeed, one must verify that the original length of the geotextile reinforcement in the resistant zone plus the corresponding change in length due to the extension must equal the total length after deformation. This condition allows the determination of a unique u_F value and thus (T, u) distributions along the reinforcement.

Since the displacement of point A of the reinforcement is led by the global failure surface of the slope, the displacement compatibility condition depends on the location of this surface. To express this condition, it has been assumed that the global slip line is a log-spiral characterised by two angular parameters θ_0 and θ_1, as shown in the companion paper. Fig. 10 shows such a line in a wall reinforced by a geotextile sheet. The reinforcement is represented before (dashed line) and after (bold-faced) deformation of soil. The upstream zone of the reinforcement includes two different parts:

- Curvilinear zone A_1B_1 corresponding to the deformed membrane. Before deformation, this zone was rectilinear and of length A_0B_0;

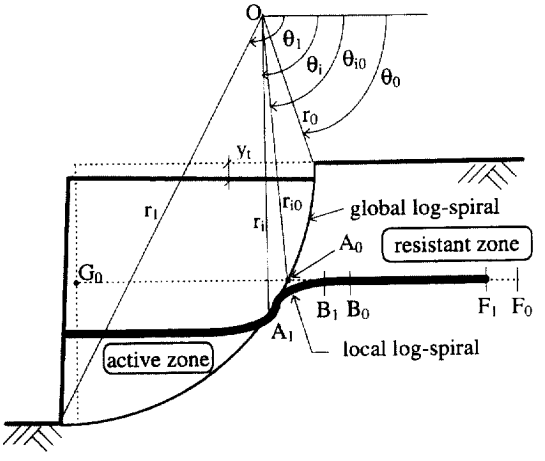

Fig. 10. Displacement compatibility.

- Rectilinear zone $\overline{B_1F_1}$ corresponding to the deformed anchorage. Before deformation, this zone was of length B_0F_0.

Let us note Δl_1 and Δl_2 the respective changes in length of zones $\overline{A_0B_0}$ and $\overline{B_0F_0}$. Thus, the displacement compatibility equation may be written as follows:

$$A_1B_1 + B_1F_1 = A_0F_0 + \Delta l_1 + \Delta l_2. \tag{18}$$

Length $\overline{B_1F_1}$ may also be expressed as follows:

$$B_1F_1 = B_1F_0 - u_F = A_0F_0 - A_0B_1 - u_F. \tag{19}$$

Substituting Eq. (19) into Eq. (18), one obtains the displacement compatibility condition:

$$u_F + A_0B_1 - A_1B_1 + \Delta l_1 + \Delta l_2 = 0 \tag{20}$$

It has been shown (Lemonnier, 1995) that Δl_2 may be expressed as a non-linear function in terms of u_F. Therefore, the unique theoretical u_F value, satisfying the compatibility condition, is reached by means of incremental calculation until Eq. (20) is satisfied. Thus, for any u_F value, one has to determine four terms: A_0B_1, A_1B_1, Δl_1 and Δl_2. These terms may be expressed with respect to (1) the angular parameters of both the global and the local log-spirals; (2) the polar co-ordinates of point A_1 (i.e. θ_i, r_i, see Fig. 10); (3) the length of the upstream anchorage zone $l_u = B_1F_1$; (4) the mechanical parameters of the soil–geotextile interface and of the inclusion: λ, J, τ_p; (5) the relative soil–geotextile displacement u_F (Lemonnier, 1995). In the following, for the purpose of clarity, Eq. (20) is reduced to $v(u_F) = 0$.

3. Computational procedure

Fig. 11 represents the flow chart giving the computational procedure to obtain the critical tension $T_{A\text{mini}}$ and its inclination α_{Am}. The design data are the soil–geotextile friction angle and adhesion (ϕ_g, c_g), the soil unit weight γ, the depth of soil over the reinforcement h_g, the vertical local displacement y_1, the tensile stiffness J of the geotextile, the initial length of the reinforcement in the upstream zone L_u, the minimal value of the rate of linear behaviour of the anchorage ta_{mini} and finally the parameters defining a particular failure surface.

Note that each u_F value corresponds, if it exists, to $T_{A\text{mini}}$ and α_{Am} values. Tension $T_{A\text{mini}}$ has to satisfy the two following conditions (see step 5, Fig. 11):

- It should not exceed the allowable tensile force to avoid failure of the reinforcement;
- It should not exceed the available adhesive and frictional forces along the reinforcement length A_1F_1 to avoid sliding of the reinforcement.

Now, a unique u_F value satisfies the displacement compatibility condition (see step 6, Fig. 11): $v(u_F) = 0$. Thus, steps 2–6 have to be executed for different u_F values until this condition is satisfied.

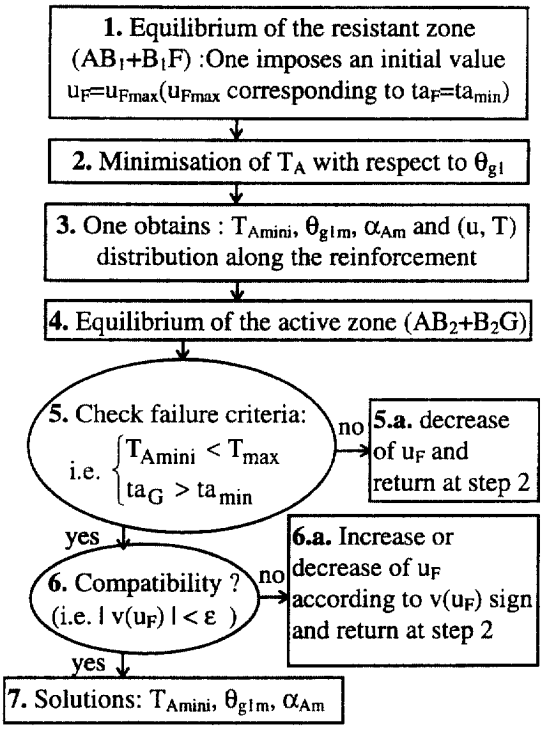

Fig. 11. Flow chart showing the calculation scheme of tension T_{Amini}.

4. Numerical results

The present theoretical analysis is now completely defined. In this section, one firstly presents a parametric study concerning a unique geotextile sheet reinforcing a vertical wall (see Fig. 12). The influence of u_F, L_u and y_1 on the determination of the reinforcement tension T_A, in case of model 4 of the σ_1 stress distribution, is presented and discussed. Then, the influence of the different assumptions (i.e. models 1–4) concerning the σ_1 stress distribution on the determination of the reinforcement tension, is presented. Secondly, a comparative case study, with results obtained from other current design methods and with some data measured *in situ*, is presented and discussed.

4.1. Parametric study

4.1.1. Influence of relative soil–geotextile displacement u_F

Fig. 13 shows the variation of T_A versus θ_{g_1} for several u_F values. It appears that for each u_F value, there is one θ_{g_1} value that realises an absolute minimum for function T_A. These numerical results confirm the theoretical ones concerning the application of

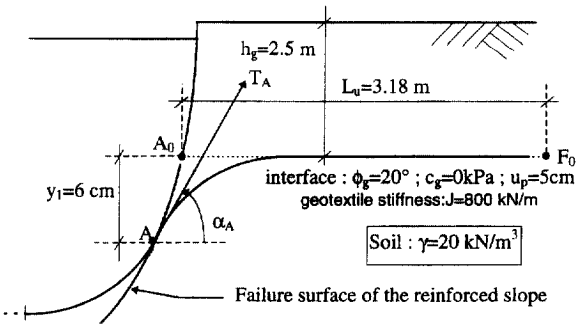

Fig. 12. Case study.

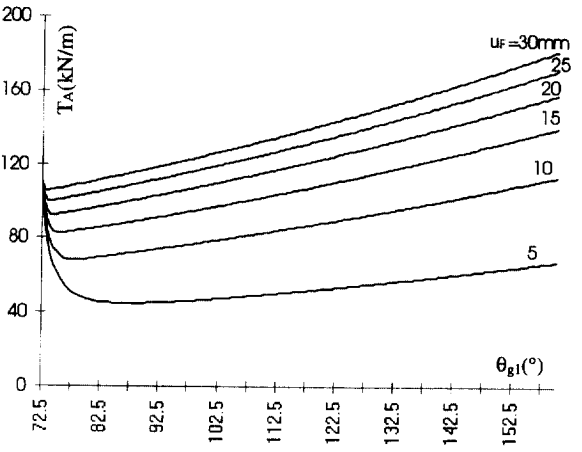

Fig. 13. Variation of T_A versus θ_{g1} for u_F = 5–30 mm (Model 4).

the variational calculus to the upstream membrane. This minimum is the critical tension T_{Amini} relative to this u_F value, and is reached at an angle u_F, which gives the optimal inclination $\theta_{g,m}$ of T_{Amini} as follows:

$$\alpha_{Am} = \theta_{g,m} + \phi_g - \frac{\pi}{2}.$$

This minimum value T_{Amini} increases, and $\theta_{g,m}$ decreases when u_F increases. That means that a greater u_F value corresponds to a lesser α_{Am} value, that is the membrane tends to become flatter.

Fig. 14 shows the influence of u_F on the location of the critical position of the upstream membrane. It clearly shows that (1) the membrane tends to become flatter as the u_F value increases; (2) T_{B_i} variation is similar to that of T_{Amini}; (3) these tensions

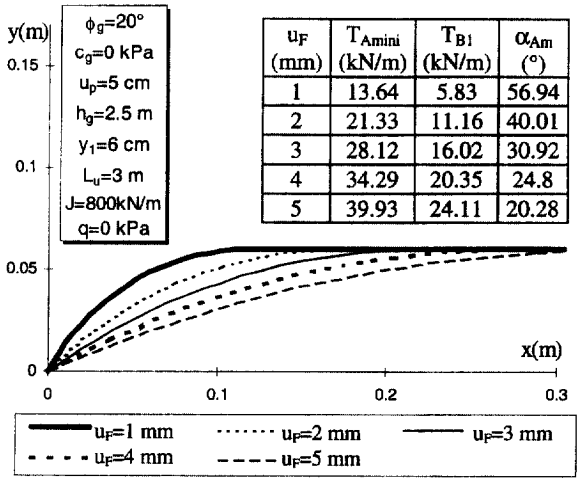

u_F (mm)	T_{Amini} (kN/m)	T_{B1} (kN/m)	α_{Am} (°)
1	13.64	5.83	56.94
2	21.33	11.16	40.01
3	28.12	16.02	30.92
4	34.29	20.35	24.8
5	39.93	24.11	20.28

Fig. 14. Critical positions of the membrane for u_F = 1–5 mm (Model 4).

increase significantly with u_F and (4) tension T_{Amini} is always greater than tension T_{B_1}. Note that point (4) concurs with the assumption concerning the location of maximum tension in the reinforcement (cf. Section 2).

4.1.2. Influence of the anchorage length in the upstream zone

Fig. 15 shows the variation of the critical position of the upstream membrane for a fixed u_F value (5 mm), the total anchorage length in the upstream zone L_u varying from 2 to 3.5 m. It shows that when L_u increases, the membrane tends to become flatter and tensions T_{Amini} and T_{B_1} increase significantly.

4.1.3. Influence of the vertical displacement of point A

In this section, the length L_u = 2.5 m is considered. Fig. 16 shows the variation of the critical position of the upstream membrane for a fixed u_F value (5 mm), the vertical displacement y_1 of point A, varying from 1 to 4 cm.

It shows that when y_1 increases, (1) the critical tension T_{Amini} increases slightly; (2) tension T_{B_1} decreases slightly; (3) α_{Am} increases; and (4) the length of the membrane increases.

4.1.4. Influence of the model of the σ_1 stress distribution

Fig. 17 represents the variation of T_{Amini} and α_{Am} versus u_F for the four proposed models of the σ_1 stress distribution. It shows that these distributions have a negligible effect on the determination of T_{Amini} for all u_F values considered. Concerning α_{Am}, there is a significant effect for small u_F values. From a particular u_F value (approximately 7 mm), the four models give quite the same results. The influence on the moment of tension T_{Amini} about the pole of the given global log-spiral has also been considered. The results, which are not presented in this paper, are very similar to these ones.

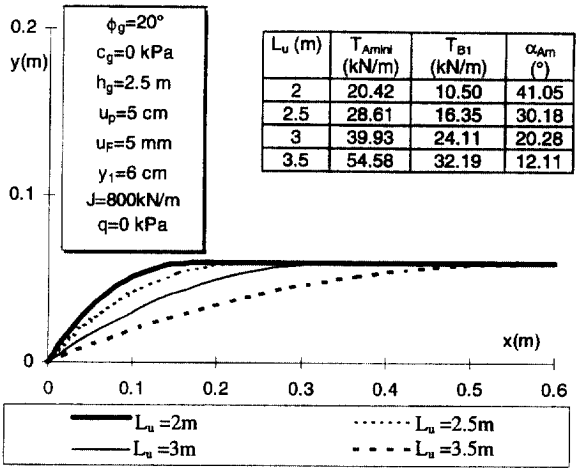

L_u (m)	T_{Amini} (kN/m)	T_{B1} (kN/m)	α_{Am} (°)
2	20.42	10.50	41.05
2.5	28.61	16.35	30.18
3	39.93	24.11	20.28
3.5	54.58	32.19	12.11

Fig. 15. Critical positions of the membrane for L_u = 2 to 3.5 m (model 4).

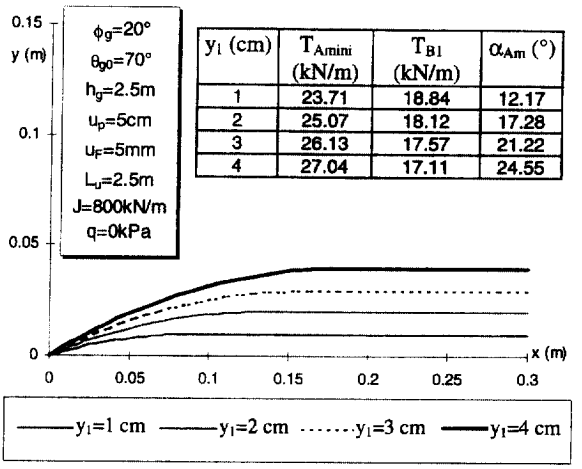

y_1 (cm)	T_{Amini} (kN/m)	T_{B1} (kN/m)	α_{Am} (°)
1	23.71	18.84	12.17
2	25.07	18.12	17.28
3	26.13	17.57	21.22
4	27.04	17.11	24.55

Fig. 16. Critical positions of the membrane for y_1 = 1–4 cm (model 4).

4.2. Comparative case study

In this section, the results obtained from the present model are compared with those obtained from some of the most current design methods available for geosynthetically reinforced slope stability analysis in the case of a large-scale model geogrid reinforced wall [presented in a paper by Bathurst et al. (1988)]. Fig. 18 shows the geometry of this wall, which is referred to as the RMC model wall (Royal Military College of Canada). The surcharge of 50 kN/m, acting on top of the wall, was the one

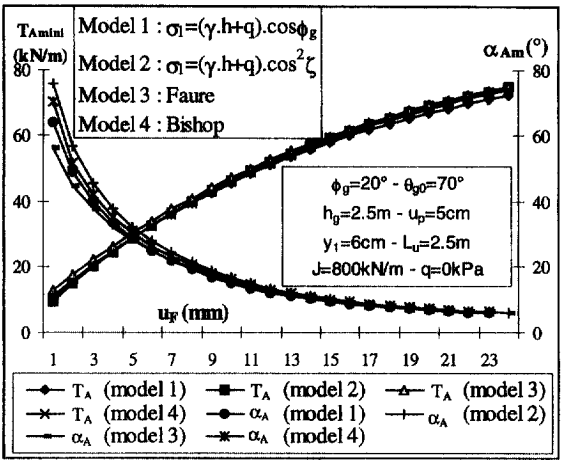

Fig. 17. Influence of the σ_1 stress distribution on T_{Amini} and α_{Am} as given by the present four models.

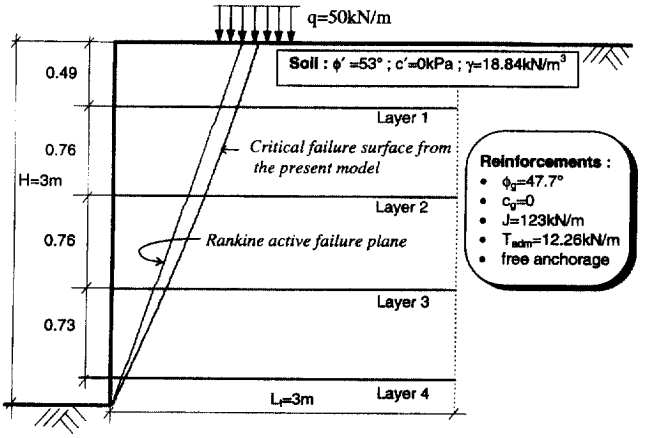

Fig. 18. RMC model wall configuration [after Claybourn (1990)], and failure surfaces considered in the design methods.

corresponding to failure. The above-mentioned current design methods were already applied to this model wall by Claybourn (1990). These methods are:

1. Forest service method (Steward et al., 1977, revised 1983);
2. Broms (1978) method;
3. Collin (1986) method;
4. Bonaparte et al. (1987) method;
5. Leshchinsky and Reinschmidt (1985) method;
6. Schmertmann et al. (1987) method.

These methods may be classified into two main groups:

1. The first one includes methods (1)–(4) (referred to as the tied-back wedge methods), which are based on lateral earth pressure considerations. That is the reinforcement tensions, which are assumed to act in the horizontal direction, balance the horizontal forces due to lateral earth pressures tending to cause instability. In these methods, a planar failure surface through the reinforced mass described by a Rankine active failure condition is typically presumed.
2. The second one includes methods (5) and (6), which are based on the approach commonly used in conventional slope stability analysis (i.e. analysis of stresses on a failure surface) modified to take into account the effect of the reinforcement tensions. Method (5) is based on a variational approach applied on limiting equilibrium analyses. Method (6) is based on limiting equilibrium analysis using wedge failure models.

Because of the significant variations among the methods, Claybourn (1990) has chosen to consider the ultimate wide width reinforcement tensile strengths and set all safety factors to 1.0. This author has then presented the results, in terms of reinforcement tensions, obtained from the different methods along with the measured reinforcement stress reported by Bathurst et al. (1988). These results, together with those obtained from the present model, are presented in Fig. 19. The latter results correspond to a particular value of the vertical displacement on top ($y_t = 19.7$ mm) for which the minimum factor of safety F_s equals 1, considering a log-spiral as failure surface (see companion paper).

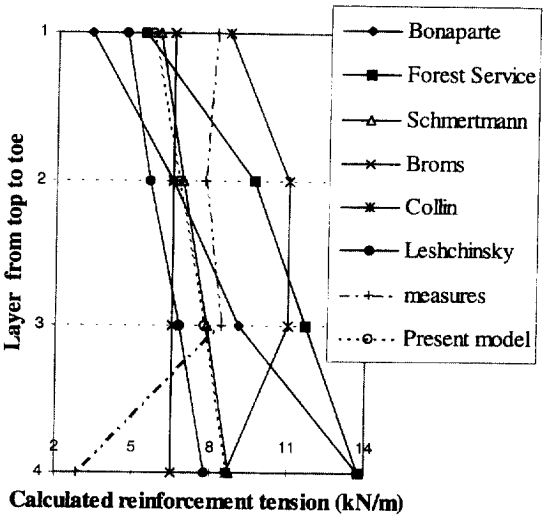

Fig. 19. Reinforced tension calculated for RMC wall configuration.

Furthermore, the limit soil/geotextile displacement u_p (cf. Fig. 9) that is required for the present model is not available in the RMC wall report. Nevertheless, the influence of this parameter on the determination of the reinforcement tension is not significant (cf. Ratel, 1987). For the present case, the value of 2.5 cm for u_p has been selected, which is a realistic value according to several experimental studies on the determination of this parameter considering granular material reinforced with geogrids (Ratel, 1987; Gotteland, 1991).

The results presented in Fig. 19 show that the present model gives similar results to those using Schmertmann et al.'s method in terms of the magnitude of the reinforcement tension distribution along the failure surface. It should be noted that, among these six methods, Schmertmann et al.'s method is (1) the only one that is specific to geogrid-reinforced soil slopes and (2) except for the lowest sheet, the one that gives the best prediction of the actual behaviour of the structure. However, the RMC Model Wall report indicated that the low bottom layer stress was probably influenced by the model set-up (Claybourn, 1990). Therefore, the comparison with the experimental data, for the fourth layer, is meaningless.

In terms of acting direction of the critical tensions, methods (1)–(6) consider it as horizontal. Furthermore, method (5) considers also the reinforcement tensions acting in the direction of the failure plane (for the Rankine active failure plane, the inclination equals 71.5° with respect to the horizontal direction). The values of these inclinations, obtained from the present model, are given in Table 1, in which the maximum inclination values correspond to the direction of the failure plane. Since the inclination of the membrane at the failure surface was not measured in this project, no comparison can be made with measured data. Nevertheless, the results from the present model show that the inclination tends to increase with the depth, and that the values are clearly smaller than the maximum one.

The obtained critical failure surface (log-spiral), shown in Fig. 18, is close to the plane described by a Rankine active failure condition, and describes a bigger sliding mass.

Finally, in the RMC wall report, an effective reinforcement length is given ($L_t \approx 1.189$ m). This is the length beyond which the performance of the wall is presumed (by the current design methods) to be unaffected by further lengthening of the reinforcement for the loading condition at failure. The effective reinforcement length obtained from the present model is slightly smaller $L_t \approx 1.07$ m (a difference of 11.6%).

Consequently, this result and the one concerning the inclination of the critical tensions show that, for this particular case, our model seems to be less conservative than the current design methods.

Table 1
Inclinations of the reinforcement tensions as given by the present model

Layer number	1	2	3	4
α_A (deg)	48.71	50.47	51.69	52.52
α_A max (deg)	72.31	70.14	68.04	66.09

5. Conclusions

All methods currently used for the design of geosynthetic reinforced slopes are based on assumptions regarding the determination of reinforcement tension. The present model is a more rational one since it allows the determination of these tensions with a reduced number of assumptions. This reduction has been made possible by the use of a variational approach together with the concept of the anchored membrane (Gourc et al., 1986). Thus, the variational calculus has been applied to the equilibrium of the upstream membrane for a given σ_1 stress distribution on its upper face (model 1). The following results have been obtained:

- the shape of the upstream membrane that realises the minimum value of T_A, is a log-spiral of angle ϕ_g with only one variable angular parameter θ_{g1};
- the critical tension $T_{A\text{mini}}$ and its inclination α_{Am} are independent of the normal stress distribution $\sigma(x)$ along the lower face of the upstream membrane $y(x)$;
- the only moment equilibrium equation about the pole of the log-spiral is sufficient to assess the tension T_A and its inclination α_A associated with this slip line. The two remaining force equilibrium equations are implicitly satisfied, because every function of the normal stress distribution $\sigma(x)$ that has at least two degrees of freedom is a solution to the problem;
- $T_{A\text{mini}}$ is obtained by an unidimensional minimisation procedure with respect to θ_{g1}.

Three other σ_1 stress distributions have been proposed. It has been shown that (1) the above results are also valid for these three models, and (2) a numerical study has shown that these four models give quite the same results for the critical tension T_j and its inclination α_j. Furthermore, the influence of the anchorage length and the vertical local displacement of the membrane on the critical position of the membrane have been shown. Finally, a comparative case study, with results obtained from other current design methods and with some data measured *in situ*, has shown that, in that particular case, our model gives (1) a satisfactory prediction of the behaviour of the reinforced structure in terms of magnitude of the reinforcement tensions, and (2) seems to be less conservative than the current design methods.

References

Baker, R., Garber, M., 1977. Variational approach to slope stability. In Proceedings of the 9th International Conference on Soil Mechanics and Foundation Engineering, Tokyo, Japan, vol. 2, pp. 9–12.

Bathurst, R.J., Benjamin, D.J., Jarrett, P.M., 1988. Laboratory study of Geogrid Reinforced Walls. In: (Ed.) R.D. Holtz. Proceedings of the Symposium on Geosynthetics for Soil Improvement, ASCE Geotechnical Special Publication, No. 18, pp. 178–192.

Blanchier, A., 1982. Etude de la stabilité d'un talus renforcé par des nappes géotextiles. PhD thesis, Université Claude Bernard Lyon I, France.

Bonaparte, R., Holtz, R.D., Giroud, J.P., 1987. Soil reinforcement design using geotextiles and geogrids. Geotextile testing and the design engineer. ASTM STP 952, pp. 69–116.

Broms, B.B., 1978. Design of fabrics reinforced retaining structures. In Proceedings of the Symposium on Earth Reinforcement. ASCE. Pittsburgh, PA, USA, pp. 282–304.

Claybourn, A.F., 1990. A comparison of design methods for geosynthetic-reinforced earth walls. MSc thesis, Department of Civil Engineering, University of Colorado, Denver, CO.

Collin, J.G., 1985. Earth wall design. Ph.D. Thesis, Department of Civil Engineering, University of California, Berkeley, CA.

Delmas, P., Gourc, J.P., Berche, J.C., 1986. Le dimensionnement des ouvrages renforcés par géotextiles programme CARTAGE. Bulletin Liaison Laboratoire des Ponts et Chaussées,, 142, 33–44.

Delmas, Ph., Gotteland, Ph., Gourc, J.P., Haidar, S., 1992. Two full size structures reinforced by geotextiles. Grouting Soil Improvement and Geosynthetics, ASCE Geotechnical Special Publication, 30(2), 1201–1213.

Faure, R.M., 1986. Analyse des contraintes dans un talus par la méthode des perturbations. Revue française de géotechnique, 33, 49–59.

Fidler, S., Gotteland, Ph., Gourc, J.P., Haidar, S., 1994. Evolution of the 'Displacement Method' applied to soil reinforced structures. In Proceedings of the Fifth International Conference on Geotextiles, Geomembranes and Related Products, Singapore, pp. 225–228.

Galera, I., 1990. Approche théorique du comportement du complexe sol-géosynthétique. PhD Thesis, Université Grenoble I, France.

Gotteland, Ph., 1991. Reinforcement des sols par géosynthétiques; dimensionnement et validation. PhD thesis, Université Grenoble I, France.

Gourc, J.P., Gotteland Ph., Delmas Ph., 1988. Design of geosynthetic retaining walls: Displacements method and Two blocks method. Comparison and charts. In: Proceedings of the International Geotechnical Symposium on Theory and Practice of Earth Reinforcement, Fukuoka, Japan, pp. 517–522.

Gourc, J.P., Ratel, A., Delmas Ph., 1986. Design of fabric retaining walls: the displacements method. In Third International Conference on Geotextiles and Geomembranes, Vienna, Austria, Session 3A/1, pp. 289–294.

Gourc, J.P., Villard, P., Matichard Y., 1992. Pull-out behaviour of reinforcements centrifuge tests and theoretical validations. In Proceedings of the International Symposium on Earth Reinforcement, Fukuoka, Japan, pp. 73–78.

Hird, C.C., 1986. Stability charts for reinforced embankments on soft ground. Geotextiles and Geomembranes, 4, 107–127.

Huisman, M.J.H., 1987. Design guideline for reinforced embankments on soft soil using Stabilenka reinforcing mats. In: Arnhem: Enka Industrial Systems, p. 38.

Kaniraj, S.R., 1994. Rotational stability of unreinforced and reinforced embankments on soft soils. Geotextiles and Geomembranes, 13 (11) 707–726.

Lemonnier, P., 1995. Application de la méthode variationnelle au problème de la stabilité des talus renforcés par des nappes géosynthétiques. Ph.D. Thesis. I.N.S.A Lyon, France.

Lemonnier, P., Soubra, A.H., Kastner, R., 1998. Variational displacement method for geosynthetically reinforced slope stability analysis: II. Global stability. Geotextiles and Geomembranes 16 (1) 27–44.

Leshchinsky, D., Reinschmidt, A.J., 1985. Stability of membrane reinforced slopes. Journal of Geotechnical Engineering, ASCE, 111 (11), 1285–1300.

Low, B.K., Wong, K.S., Lim, C., Broms, B.B., 1990. Slip circle analysis of reinforced embankments on soft ground. Geotextiles and Geomembranes, 9, 165–181.

Ratel, A., 1987. Modélisation d'un sol reinforcé par géosynthétique: application de la 'méthode en déplacements'. PhD thesis, Université Scientifique et Médicale et l'Institut National Polytechnique de Grenoble, France.

Schmertmann, G.R., Chouery-Curtis, V.E., Johnson, R.D., Bonaparte, R., 1987. Design charts for geogrid reinforced soil slopes. In: Proceedings of Geosynthetics '87, New Orleans. IFAI, pp. 108–120.

Steward, J.E., Williamson, R., Mohney, J., 1977. Guidelines for use of fabrics in construction and maintenance of low-volume roads. In Chapter 5: Earth Reinforcement, USDA, Forest Service, Portland, OR, revised 1983, pp. 87–95 and 102–105.

Yoshioka, A., Delmas, Ph., Gourc, J.P., Gotteland, Ph., 1990. Validation of the 'Displacements Method' on an experimental reinforced wall at failure. In: Proceedings of the Fourth International Conference on Geotextiles, Geomembranes and Related Products, The Hague, The Netherlands, pp. 61–66.